

Multi-Angle Implementation of Atmospheric Correction for MODIS (MAIAC).

Part 3: Atmospheric Correction

A. Lyapustin, Y. Wang, I. Laszlo, T. Hilker, F. Hall, P. Sellers, J. Tucker, S. Korkin

Abstract. This paper describes the atmospheric correction (AC) component of the Multi-Angle Implementation of Atmospheric Correction algorithm (MAIAC) which introduces a new way to compute parameters of the Ross-Thick Li-Sparse (RTLS) Bi-directional reflectance distribution function (BRDF), spectral surface albedo and bidirectional reflectance factors (BRF) from satellite measurements obtained by the Moderate Resolution Imaging Spectroradiometer (MODIS). MAIAC uses a time series and spatial analysis for cloud detection, aerosol retrievals and atmospheric correction. It implements a moving window of up to 16 days of MODIS data gridded to 1 km resolution in a selected projection. The RTLS parameters are computed directly by fitting the cloud-free MODIS top of atmosphere (TOA) reflectance data stored in the processing queue. The RTLS retrieval is applied when the land surface is stable or changes slowly. In case of rapid or large magnitude change (as for instance caused by disturbance), MAIAC follows the MODIS operational BRDF/albedo algorithm and uses a scaling approach where the BRDF shape is assumed stable but its magnitude is adjusted based on the latest single measurement. To assess the stability of the surface, MAIAC features a change detection algorithm which analyzes relative change of reflectance in the Red and NIR bands during the accumulation period. To adjust for the reflectance variability with the sun-observer geometry and allow comparison among different days (view geometries), the BRFs are normalized to the fixed view geometry using the RTLS model. An empirical analysis of MODIS data suggests that the RTLS inversion remains robust when the relative change of geometry-normalized reflectance stays below 15%. This first of two papers introduces the algorithm, a second, companion paper illustrates its potential by analyzing MODIS data over a tropical rainforest and assessing errors and uncertainties of MAIAC compared to conventional MODIS products.

1. Introduction

The measured top of atmosphere (TOA) radiance is a function of both aerosol properties and surface bidirectional reflectance, and separating their contributions has been one of major obstacles for retrieval of accurate surface reflectance. The current operational MODIS aerosol algorithm MOD04 uses the Dark Target method (Kaufman et al., 1997; Remer et al., 2005; Levy et al., 2007) which relies on an empirical spectral regression coefficient (SRC) to define the relationship between the visible and shortwave IR (SWIR, 2.1 μm) surface reflectance. This SRC is optimized for vegetated and dark land surfaces where aerosols are retrieved with high accuracy. The lack of retrievals over bright surfaces, however, and correlation between aerosol optical thickness (AOT), retrieved at high spatial resolution, and surface brightness over heterogeneous, especially urban, surfaces (e.g., Remer et al., 2005; Lyapustin et al., 2011b), are known limitations of the current MODIS approach. A version of the Dark Target method has been implemented in the Collection 5 MODIS Atmospheric Correction (AC) algorithm MOD09 (Vermote and Kotchenova, 2008). This algorithm makes aerosol retrievals at MODIS pixel resolution, and further derives surface reflectance using Lambertian assumption. Besides limitations of the Dark Target method, the MOD09 surface reflectance has relatively small but non-negligible biases from the use of the Lambertian surface model, which grow with aerosol loading, atmospheric mass and inverse wavelength (Wang et al., 2010; Pinty et al., 2011).

This paper describes the Multi-Angle implementation of Atmospheric Correction algorithm (MAIAC) which retrieves parameters of the bidirectional reflectance distribution function (BRDF) model from the time series of MODIS measurements along with spectral albedo and BRDF without Lambertian assumption. The MAIAC cloud mask and aerosol algorithms were described earlier (Lyapustin et al., 2008, 2011b). Due to retrieval of SRC, MAIAC provides aerosol information at high spatial resolution of 1 km over both dark and moderately bright surfaces in a uniform manner. The AC algorithm also uses MAIAC cloud mask and column water vapor (Lyapustin and Wang, 2009).

Below, section 2 gives an overview of the implemented time series processing and structure of the MAIAC queue storing multi-day information for the sliding window algorithm. Section 3 describes the atmospheric correction algorithm, discusses the problem of seasonal and rapid surface change, and introduces the suite of MAIAC surface reflectance products. Section 4 gives several examples of MAIAC processing from the small- and large-scale analysis. Lastly, section 5 gives final considerations of merits and limitations of the developed time series approach.

Previously, MAIAC was successfully tested in applications which demand very high accuracy of atmospheric correction, such as Photochemical Reflectance Index (PRI) analysis (Hilker et al., 2009, 2010). The detailed validation of MAIAC land surface products using the AERONET-based Surface Reflectance Validation Network (Wang et al., 2009) will be given elsewhere. A rather comprehensive analysis of the MAIAC land products, focused on analysis of vegetation greenness, and comparison with equivalent MODIS operational products for the Amazon region is presented in the companion paper (Hilker et al., this issue).

2. Implementation of the Time Series Processing

The core of MAIAC processing is a sliding window algorithm which holds between 5 (at the poles) and 16 (at the equator) days of imagery, depending on latitude, with up to 80 observations. MAIAC processing starts by gridding the received MODIS calibrated and geolocated (L1B) data (Wolfe et al., 1998), splitting them into tiles, and placing the new data in the processing queue with the previous data. Given the selected projection, the gridding process translates sensor's geolocated swath observations into grid cells of fixed lat-lon coordinates. In order to limit variation of the footprint with changing view zenith angle (VZA), the resolution of MODIS 500m channels B1-B7 is coarsened to 1 km. The MAIAC processing uses both individual grid cells, also called pixels below, and fixed-size ($25 \times 25 \text{ km}^2$) areas, or blocks, required by the cloud mask, surface change and aerosol algorithms. To organize such processing, we developed a framework of C++ classes and structures (algorithm-specific Containers). The class functions are designed to handle processing in the various time-space scales, for example at the pixel- vs block-level, and for a single (last) day of measurements vs all available days in the queue, or for a subset of days which satisfy certain requirements (filters).

The structure of the MAIAC processing Queue is shown schematically in Figure 1. For every day of observations, MODIS measurements are stored as layers for reflective bands 1-13 for the AC algorithm. The queue stores the retrieval results required for atmospheric correction, such as water vapor and aerosol information. Besides storing gridded MODIS data (tiles), the queue has a dedicated memory (Q-memory) which accumulates ancillary information about every block and every pixel of the surface for the cloud mask algorithm. It also keeps information related to the history of previous retrievals, for example parameters of spectral BRDF model and albedo,

which are required for both aerosol and AC algorithms. Given the daily rate of MODIS observations, the land surface represents a relatively stable background over short time intervals. Therefore, knowledge of the previous surface state significantly enhances the accuracy of aerosol retrievals and cloud detection, as well as the quality of atmospheric correction, for example, by imposing a requirement of consistency of the time series of BRDF and albedo.

Because MAIAC memory requirements are high, the size of the tile can be scaled to fit an operational memory of a particular workstation (e.g., 300-1000 km) with the constraint that it should be a multiple of the block size (25 km).

3. Atmospheric Correction

The MAIAC cloud mask algorithm has been described in detail in Lyapustin et al. (2008). Briefly, the algorithm composes a dynamically updated reference clear-sky image of the surface from spatial and time series analyses. The knowledge of reference clear-sky reflectance in addition to spectral and thermal reflectance tests (Ackerman et al., 1998) has been shown to improve cloud detection considerably (Lyapustin et al., 2008). Once the cloud mask is created and aerosol retrievals performed, the time series of MODIS measurements is filtered for every pixel and the remaining clear-sky data are placed in a “container”. The filter excludes pixels with clouds and cloud shadows, the snow-covered pixels as detected by the CM algorithm during land-water-snow classification (see Lyapustin et al., 2008), and pixels with high AOT (>1) where sensitivity of measurements to surface reflectance is low. The container stores measurements along with the corresponding radiative transfer functions from the look-up table (LUT). If the number of available measurements exceeds 3 for a given pixel with sufficient angular coverage, then the coefficients of BRDF model are computed.

3.1 Inversion for RTLS Coefficients

In the operational MODIS land processing, the BRDF is determined in two steps: first, the atmospheric correction algorithm derives surface reflectance for a given observation geometry in Lambertian approximation (Vermote and Kotchenova, 2008), and next, parameters of the Ross-Thick Li-Sparse (RTLS) model (Lucht et al., 2000) are retrieved from the time series of surface reflectance accumulated for a 16-day period (Schaaf et al., 2002). The retrieval is currently repeated once every 8 days.

The RTLS model is also used in MAIAC. This is a linear kernel model depending on three k -coefficients used to describe isotropic (or Lambertian), volumetric (Roujean et al., 1992) and geometric-optical (Li and Strahler, 1992) terms:

$$\rho(\mu_0, \mu, \varphi) = k^L + k^V f_V(\mu_0, \mu, \varphi) + k^G f_G(\mu_0, \mu, \varphi). \quad (1)$$

The MAIAC AC algorithm derives RTLS coefficients directly by fitting the measured TOA reflectance accumulated for a period of 4-16 days. The inversion is based on equation (25) derived in (Lyapustin et al., 2011a):

$$R(\mu_0, \mu, \varphi) = R^D(\mu_0, \mu, \varphi) + k^L F^L(\mu_0, \mu) + k^V F^V(\mu_0, \mu, \varphi) + k^G F^G(\mu_0, \mu, \varphi) + R^nl(\mu_0, \mu). \quad (2)$$

Here, R^D is atmospheric (path) reflectance and F -functions are integrals of the atmospheric path radiance incident on surface and atmospheric Green's function (Lyapustin and Knyazikhin, 2001) with respective kernels of the RTLS model. R^nl is a weakly non-linear function of the surface

reflectance, describing multiple light scattering between the surface and atmosphere. The F -functions and R^{nl} are computed analytically using eight primary functions which are stored in the look-up table (LUT). The fast LUT radiance-restore algorithm computes the TOA reflectance as a function of view geometry, wavelength, surface pressure, column water vapor and aerosol parameters (optical thickness and aerosol model) (Lyapustin et al., 2011a).

Equation (2) provides an explicit parameterization of the TOA reflectance in terms of the RTLS BRDF model parameters $\vec{K} = \{k^L, k^G, k^V\}^T$. The quasi-linear form of equation (2) leads to a very efficient iterative minimization algorithm:

$$rmse = \sum_j (r_j^{(n)} - F_j^L k^{L(n)} - F_j^V k^{V(n)} - F_j^G k^{G(n)})^2 = \min_{\{\vec{K}\}}, r^{(n)} = R - R^D - R^{nl(n-1)}, \quad (3)$$

where R is measured reflectance, index j refers to different days, and n is the iteration number. Equation (3) provides an explicit least-squares solution for the kernel weights. In matrix form, the solution is written as:

$$\vec{K}^{(n)} = A^{-1} \vec{b}^{(n)}, \quad (4)$$

where

$$A = \begin{bmatrix} \sum_j (F_j^L)^2 & \sum_j F_j^G F_j^L & \sum_j F_j^V F_j^L \\ \sum_j F_j^G F_j^L & \sum_j (F_j^G)^2 & \sum_j F_j^V F_j^G \\ \sum_j F_j^V F_j^L & \sum_j F_j^V F_j^G & \sum_j (F_j^V)^2 \end{bmatrix}, \quad \vec{b}^{(n)} = \begin{bmatrix} \sum_j r_j^{(n)} F_j^L \\ \sum_j r_j^{(n)} F_j^G \\ \sum_j r_j^{(n)} F_j^V \end{bmatrix}.$$

In the first iteration, the small non-linear term is set to zero, $R_j^{nl(0)} = 0$, and the multiple reflection factor α (see Lyapustin et al., 2011a) is set to one, $\alpha^{(0)} = 1$. These parameters are updated once, after the RTLS coefficients are computed in the first iteration. Except for snow-covered surfaces, the convergence is achieved with high accuracy in two iterations in all conditions because the non-linear terms are small.

Prior to inversion, the algorithm checks if the dataset has a sufficient angular sampling. This issue was investigated in several studies (e.g., Barnsley et al., 1997; Lucht and Lewis, 2000). The MODIS operational BRDF/albedo algorithm (Schaaf et al., 2002) makes an inversion if at least 7 cloud-free observations are available during the 16-day period. Except for the dry arid regions of the world, this condition cannot easily be met. To increase frequency of retrievals, we studied the inversion problem experimentally with MODIS data varying the minimal number of measurements n (from 3 to 10) and testing different metrics of angular sampling. One of the metrics tested was the determinant of the inverse matrix A which indicates whether the sampling angles are sufficiently different for model inversion. Although such analysis is, perhaps, most straightforward theoretically, we found it often too restrictive. In the end, a simple criterion was chosen based on the range of cosine of the view zenith angle ($\mu_{\max} - \mu_{\min} \geq 0.2$) and a requirement that the measurements in both forward and backscattering range of angles are represented, which is usually sufficient for a robust and consistent retrieval at $n \geq 4$.

3.2 Solution Selection and Update

Although the RTLS model allows efficient inversion due to its linearity, there are several caveats associated with this model. First, the RTLS kernels are not orthogonal, are not positive-only functions, and are normalized in a somewhat arbitrary fashion that is not linked to the radiative transfer. These factors reduce the stability and uniqueness of the solutions, such that small perturbations in measurements may lead to significantly different solutions in terms of k -coefficients. Second, the high goodness-of-fit at the measurement angles alone does not guarantee the correct shape of the retrieved BRDF, and may result in negative or very large positive BRF values at other angles. The albedo, being an integral function, is especially sensitive to the BRDF shape. For these reasons, we use several tests to remove the unrealistic solutions.

The initial validation of the solution checks that the maximal difference over all days between the measured and computed TOA reflectance does not exceed a threshold of 0.05, $|R^{Meas} - R^{RTLS}| \leq 0.05$. If it does, the day (measurement) with the highest deviation is excluded from the queue and the inversion is repeated.

In the next test, the algorithm verifies that values of the direct-beam albedo (q) at $SZA=15^\circ$, 45° , 65° are positive and that the new solution is consistent with the previous solution: $|q(45^\circ) - q^{Prev}(45^\circ)| < \Delta(\lambda)$, where Δ is the band-dependent threshold currently equal to 0.04 (blue), 0.05 (green and red), 0.07 (for spectral region of 0.8 – 1.6 μm) and 0.05 for the shortwave infrared band (2.1 μm). Consistency of the solution is characterized by a *status* index. Initially, the confidence in the solution is low (*status*=0). Each time the new retrieval agrees with the previous retrieval, *status* increases by 1. When *status* ≥ 3 , the RTLS solution is considered reliable.

The thresholds (0.05 and $\Delta(\lambda)$) in the RTLS inversion routine are selected to be strict enough to reject most of undetected clouds which remain the dominant source of errors, but sufficiently loose for the solution to adapt to potential surface change. The most pervasive type of change is seasonal variations, related to the spring green-up and fall senescence at northern latitudes, or greenness variations caused by wet and dry seasons in tropics. The total seasonal variation of reflectance over vegetated surface is about several absolute percent in the visible bands (~ 0.03 - 0.1), and is significantly higher in the near infrared (~ 0.1 - 0.4). The threshold $\Delta(\lambda)$ for the daily variation was selected accordingly, and our analysis of a large volume of processed MODIS data confirms that the MAIAC algorithm does not reject measurements when surface is changing, even in the agricultural regions characterized by the rapid reflectance change during green-up or harvesting.

When the new solution is validated, the RTLS coefficients and direct-beam albedo $q(45^\circ)$, stored in the Q-memory, are updated. The update is done with relaxation, designed to mitigate the random noise of retrievals:

$$\vec{K}_\lambda = w \vec{K}_\lambda^{New} + (1-w) \vec{K}_\lambda^{Prev}. \quad (5)$$

The weight w depends on our confidence in the previous solution, which increases with its *status*. The weight $w=1$ for the first retrieval (*status*=0), $w=0.8$ for the second retrieval, $w=0.6$ for the third consecutive retrieval, and $w=0.5$ thereafter. This method of update reduces random

noise when the surface is relatively stable, but it delays response when the surface is changing. To avoid the solution response delay, the status of the pixel is dropped to unity when the seasonal (low amplitude) change is detected, or to zero in case of detected rapid (high amplitude) change (see sec. 3.3).

When the solution cannot be produced because of cloudiness or high atmospheric turbidity, we assume that the surface remains stable and the gaps can be filled with the previous RTLS solution for up to a 32-day period. During the short time intervals (1-4 weeks) when the surface is not expected to change, this is the most natural and accurate way of gap-filling with specific RTLS/albedo spectral solution for a given pixel, which does not involve additional assumptions. On the other hand, the gap-filling methods based on the land cover classification and other ancillary information (e.g., *Moody et al.*, 2008), may provide an alternative extrapolation for the longer time periods. For the user's decision support, the gap-filled pixels are marked as "Extended" in the quality assurance (QA) value, with parameter *QA.nDelay* giving the number of days since the last update.

3.3 Accommodation of Surface Change

The AC algorithm described above works well when the rate of surface change is not high, or in other words, when the change in surface reflectance during the 16-day period does not exceed a certain threshold. In this case, the AC algorithm adjusts the RTLS model parameters in a timely fashion, as for example over the East Coast USA. On the other hand, in regions with strong vegetation dynamics and bright soils, e.g. USA mid-West agricultural regions, the surface albedo change in 16-day intervals may be very high. In general, the RTLS inversion during the period of surface change is not a valid procedure, as changes in reflectance over time are attributed to the particular observation angles and BRDF shape. In general, the question of how much the surface can change with retrievals still providing a reasonable BRDF shape, remains unanswered. For example, the MODIS operational BRDF/albedo algorithm adopted an empirical approach where the RTLS model inversion is attempted each time, and when it fails, the scaling algorithm is applied. In the last case, the magnitude of reflectance is adjusted (scaled) with the single last measurement assuming that the BRDF shape does not change significantly with the surface change.

In the current MAIAC version, the change detection algorithm is triggered when the atmosphere is not hazy ($AOT_{0.47} < 0.4$ globally, and < 0.6 for regions with perpetual haze, e.g. Indo-Gangetic plane). The change detection is based on the Red and NIR MODIS bands (1-2), and requires synchronous change in both bands in the opposite directions, for example decrease in Red and increase in NIR for green-up, and opposite change for senescence. This approach is less prone to errors from undetected clouds as opposed to use of the normalized difference vegetation index (NDVI). To remove geometry variations and enable reflectance comparison between different days (obtained in different view geometries), we are using the geometry-normalized BRF_n :

$$\rho_n = \rho(\theta_0, \theta, \varphi) \frac{RTLS(45^\circ, 0^\circ)}{RTLS(\theta_0, \theta, \varphi)} \quad (6)$$

An example comparing BRF (see sec. 3.4) and BRF_n is given in Figure 2 for a single 1 km pixel, covered by a forest, near Greenbelt, Maryland, USA. One can see that this approach reduces geometric variability by a factor of 3-6, and parameter BRF_n shows strong seasonal cycles,

which closely resemble vegetation phenological cycles (examples for rapid surface change are given in the next section).

Using the BRF_n metric, we were able to answer the question of RTLS inversion during the period of change. Based on empirical analysis of MODIS data over different geographical locations, we found that the RTLS retrieval remains reasonable (does not produce BRDF shape artifacts, and k -coefficients change consistently during the period of change) if relative BRF_n change during the accumulation period does not exceed $\sim 15\%$,

$$\Delta\rho_n / \rho_n < 0.15. \quad (7)$$

According to this criterion, MAIAC has two values of change mask, `_CHANGE` for gradual changes of $0.05 < \Delta\rho_n / \rho_n < 0.15$, and `_CHANGE_BIG` for abrupt, larger changes of $\Delta\rho_n / \rho_n > 0.15$. In the latter case, MAIAC uses only a scaling approach where the parameters of RTLS model are scaled so that the model would match the latest measurement. Such an approach has advantages of immediate adjustment of spectral BRDF to the surface change and faster computations, assuming the BRDF shape has only a secondary role.

The detected change for individual pixels is accepted only in case of green-up which produces a spectrally unique signal. On the contrary, because the senescence signal can be confused with effect of unresolved clouds, it is only accepted if it is a large scale event covering at least a quarter of pixels in the $25 \times 25 \text{ km}^2$ block.

3.4 MAIAC Surface Reflectance Products

MAIAC computes three main land products at 1 km resolution - the set of RTLS coefficients, albedo and BRF in MODIS bands 1-8 and 12-13.

The albedo is defined in the MAIAC algorithm as ratio of surface-reflected to incident radiative fluxes (Lyapustin et al., 2011a). Thus, albedo is derived for a given solar zenith angle in ambient atmospheric conditions, and can be directly compared to ground-based measurements. Given the k -values of the RTLS model, the so-called black-sky and white-sky albedos (Schaaf et al., 2002), representing the hemispheric integrals from RTLS over the downward and downward and upward directions, respectively, under the assumption of uniform diffuse irradiance, can be easily calculated. MAIAC also internally computes a Normalized BRF for a fixed geometry of nadir view and $SZA=45^\circ$ (NBRF):

$$NBRF_\lambda = k_\lambda^L - 1.10003k_\lambda^G - 0.04578k_\lambda^V. \quad (8)$$

NBRF is analogous to the MODIS NBAR (nadir BRF-adjusted reflectance) product (part of the MOD43 standard product suite) with an additional solar angle normalization. The spectral NBRF is essentially a background image of the surface useful for the product quality analysis and imagery applications. With the geometry variations removed, the NBRF is a useful metric for different applications, and users can easily compute it from Eq. (6) using provided RTLS kernel weights.

The BRF by definition (e.g., see Schaepman-Strub et al., 2006) represents a reflectance which would be measured if the atmosphere were absent. It is produced by the MODIS operational atmospheric correction algorithm (MOD09) using Lambertian surface model and is commonly called *surface reflectance*. MAIAC computes BRF from the latest MODIS measurement using

the known BRDF shape. To illustrate computation of the BRF, we re-write equation for the measured TOA reflectance as follows:

$$R(\mu_0, \mu, \varphi) = R^D(\mu_0, \mu, \varphi) + cR^{Surf}(\mu_0, \mu, \varphi), \quad (9)$$

where R^{Surf} is a surface-reflected terms computed using the current RTLS parameters and retrieved aerosol data, and c is spectrally-dependent scaling factor. Then,

$$BRF_\lambda(\mu_0, \mu, \varphi) \cong c_\lambda RTLS_\lambda(\mu_0, \mu, \varphi), \quad (10)$$

where $RTLS_\lambda$ for the direct-beam geometry is computed from the model. Because R^{Surf} is a non-linear function of the surface reflectance, equation 10 is not rigorous. Yet, because the non-linearity is weak and scaling factor c is close to 1, the accuracy of (9-10) is high, within a few percent of the modelled values under most circumstances. The described scaling algorithm was selected in favor of an accurate computation of BRF from the direct surface-reflected term in order to account for variations of the MODIS footprint with the scan angle. Over heterogeneous surfaces, such variations can modulate the surface brightness regardless of its BRDF, and scaling algorithm (9-10) accounts for these variations symmetrically in the direct and diffuse surface-reflected terms providing overall more stable result. The BRF is computed for the land pixel if its RTLS parameters are known, the pixel is cloud-free and the atmosphere is not very hazy ($AOT < 1$).

A Lambertian assumption is used during the algorithm initialization period which may last from just 4 days in cloud-free low AOT conditions to over a month depending on cloudiness. During this period of time, the total algorithm performance is sub-optimal with higher rate of undetected clouds and reflectance biases from Lambertian assumption. In the near future, this limitation will be removed with automated re-run of the initialization period.

In addition to 1 km scale, the spectral BRF in MODIS bands 1-7 is also computed at 500m resolution from data gridded to 500m mesh nested in 1km grid. The higher resolution BRF product is required in different applications such as land disturbance/recovery or change detection. The computation uses the same scaling approach given by equations (9-10), and assumes that the BRDF shape, known at 1 km scale, is also valid at 500m resolution. Obviously, over heterogeneous surfaces this product is much more affected by the surface spatial variability than the 1km product from the pure gridding prospective. This disadvantage, however, is outweighed by the benefits of higher resolution for variety of applications.

4. Examples

In this paper, only a few examples for atmospherically corrected MAIAC data are shown as the companion paper (Hilker et al., this issue) contains an extensive comparison to conventionally atmospherically corrected MODIS data over 2.88 mill. km² of tropical rainforest. Figure 2 shows a time series of surface reflectance and NDVI from MODIS Aqua data for a single 1km pixel representing mixed forest near Greenbelt, Maryland, USA. The BRF (top) and BRF_n (middle) data are shown for 5 spectral bands: the red (B1), blue (B3) and green (B4) channels are indicated by their color, while NIR (B2) and SWIR (B7) are displayed in brown and black, respectively. To illustrate variability of BRF with changing view geometry, the data points for the NIR channel are connected by a line which shows the range of variation of 0.1-0.15 at the mean value of 0.35 during the maximum greenness. The BRDF normalization to the standard

view geometry (middle) shows a significant reduction of geometric variability, by a factor of 3-6 for different channels. After normalization, a consistent annual pattern of reflectance becomes apparent even in the dark visible channels, for example a much higher seasonal variation of chlorophyll-related blue and red band reflectances as compared to the green reflectance. This is clearly visible in the BRF_n time series plot (middle) while largely masked by geometric variations in the BRF (top) plot. The bottom plot shows that geometric normalization, at least during the summer season, has little effect on NDVI, where NDVI is shown in red and $NDVI_n$ is shown in black. In winter, the normalization reduces the NDVI variability which is mostly caused by a residual snow. Several low NDVI outliers during the maximum greenness period shows the effect of undetected clouds, although their occurrence is generally low.

Figure 3 gives an illustration of MAIAC performance using 50 km MODIS Aqua subsets for the GSFC site (Greenbelt, Maryland). This figure is a typical example of our data visualization in a form of time series, similarly to the data arrangement in the processing queue. It helps us analyze both the overall quality of solution and complex relationships between different retrieved parameters. Each image in Figure 3 shows 15 days of observations in 6 different columns: 1 - gridded MODIS Aqua TOA RGB images; 2 - MAIAC cloud mask; 3 - RGB NBRF; 4 - RGB BRF; 5 - MAIAC AOT at $0.466 \mu\text{m}$ with values in scale of 0-1; 6 - detected change. The blue and green colors in the change column indicate `_CHANGE` and `_CHANGE_BIG` greening, while the light blue and yellow colors stand for `_CHANGE` and `_CHANGE_BIG` browning.

Normally, spectral BRF captures the surface change immediately while the RTLS model response through a regular inversion process may be delayed by several days. However, with detection of a big change, the implemented scaling algorithm adjusts the BRDF model immediately based on a single day of observations. This is illustrated in the left-hand image which shows results during spring green-up (DOY 92-105, 2010). While the greening change, indicated by a blue color, is detected from the first day, the color adjustment of the NBRF which represents the BRDF model, takes place on days 10-11 with detection of `_CHANGE_BIG` greening. A similar pattern can be seen in the right image showing days DOY 285-311, 2003 during the fall senescence. Of 30 in total, the middle 15 observations are excluded as mostly covered by clouds. The `_CHANGE_BIG` browning signal, indicated by yellow, is detected in the last half of the shown period.

Figure 4 shows the difference in response of the BRDF model (via NBRF) and BRF to a rapid surface change caused by an agricultural fire near Skukuza site, Africa. The burning takes place in the upper-left corner of the images with affected area marked by ovals. The burnt area rapidly expands during the first three days which is clearly visible in the BRF image. The change detection algorithm detects change, curiously, as `_CHANGE_BIG` greening event on day 4, with scaling adjustment of the BRDF model clearly visible on day 5. This example is a demonstration of potential of MAIAC surface reflectance products complemented with change detection mask for analysis of rapid surface change and disturbance (e.g., Roy et al., 2002).

Figure 5 gives example of the large-scale MAIAC processing, showing central-eastern USA for September 19, 2007 at 10% of the original 1km resolution. Shown from top are the TOA RGB MODIS Aqua image, MAIAC cloud mask, $AOT_{0.466}$, and finally, RGB BRF and NBRF. The images stitches three MODIS granules. The change of view geometry across the border of granules is clearly visible in both TOA RGB and BRF images. The NBRF image is computed from the known RTLS BRDF model for the fixed view geometry, and shows the entire gap-free

land surface area. The above examples show the high overall quality of MAIAC processing including cloud detection and correction of atmospheric effects.

5. Concluding Remarks

This paper is third in a series of recent MAIAC publications, describing the atmospheric correction algorithm, with the radiative transfer basis and aerosol algorithm reported recently (Lyapustin et al., 2011a,b). MAIAC is an attempt to build the algorithm with physical/mathematical model of the atmosphere-surface radiative transfer as complete as possible and to provide a radiatively consistent suite of atmosphere-surface properties. On one hand, this allows us to avoid using common assumptions, for example, about the spectral regression coefficient required for aerosol retrievals, and derive it from the time series and spatial analysis of MODIS data. The synergistic nature of MAIAC and information sharing among CM, water vapor, aerosol and surface reflectance algorithms benefits the overall quality of the product suite (see a companion paper). For example, aerosol algorithm requires spectral surface BRDF information, while also providing enhanced cloud detection (Lyapustin et al., 2012). On the other hand, explicit use of the time series and a dynamic nature of the Earth reflectance increase complexity of the algorithm as it requires tracking surface state and detecting seasonal and rapid surface change for every grid cell, which we described in this paper.

Contrary to the current MODIS operational approach, where processing is split into the AC algorithm (MOD09) providing Lambertian surface reflectance and BRDF/albedo algorithm (MOD43) retrieving coefficients of RTLS model from 16 days of Lambertian reflectances, MAIAC derives BRDF coefficients directly from the time series of MODIS top of atmosphere data, along with spectral surface albedo and BRF.

The surface change detection in MAIAC is based on geometry normalized BRF_n in the Red and NIR bands. The normalization to the standard view geometry of $VZA=0^\circ$ and $VZA=45^\circ$ in BRF_n strongly suppresses geometric variations of BRF by a factor of 3-6, allowing reliable change detection. One of findings of this work establishes the empirical bounds for the spectral reflectance change during the accumulation period ($\Delta BRF_n/BRF_n < 15\%$) when the RTLS inversion remains a generally robust procedure. When the relative reflectance change is larger, the AC algorithm utilizes the MOD43 scaling approach by adjusting the magnitude of BRDF based on a single latest measurement.

MAIAC provides a gapless BRDF/albedo product: under cloudy conditions, it fills any given grid cell with the previous retrieval value for up to 32-day period assuming that the surface did not change, which is the most natural way of gap-filling with the pixel-specific values without additional assumptions.

Because MAIAC uses a block-level processing for the SRC and aerosol retrievals (Lyapustin et al., 2011b), those blocks may show in the atmospherically corrected imagery at 25 km scale. Generally, this is a minor phenomenon with magnitude within 0.001-0.002 in reflectance units in the Blue-Green bands, which rapidly decreases with wavelength. However, sometimes it becomes apparent because our eye is trained to catch geometrically correct and reproducible patterns.

Currently, MAIAC undergoes operational code conversion and testing phase. According to the current schedule, it will be used to process the full MODIS Terra and Aqua dataset using

MODIS Adaptive Processing System (MODAPS) after completion of the MODIS Collection 6 land discipline re-processing (late fall 2012 - winter 2013).

REFERENCES

- Barnsley, M., D. Allison and P. Lewis (1997). On the Information Content of Multiple View Angle (MVA) Images, *Int. J. Rem. Sens.*, 18(9), 1937-1960.
- Hilker, T., A. Lyapustin, F. G. Hall, Y. Wang, N. C. Coops, G. Drolet, & T. A. Black, 2009: An assessment of photosynthetic light use efficiency from space: Modeling the atmospheric and directional impacts on PRI reflectance. *Rem. Sens. Environment*, **113**, 2463-2475, doi:10.1016/j.rse.2009.07.012.
- Hilker, T., Hall, F., Coops, N.C., Lyapustin, A., Wang, Y., Nesic, Z., Grant, N., Black, T.A. Wulder, MA., Kljun, N., Hopkinson, C., Chaser, L., 2010: Remote sensing of photosynthetic light-use efficiency across two forested biomes: Spatial scaling. *Rem. Sens. Environ.*, 114, 2863-2874.
- Kaufman, Y. J., D. Tanre et al. (1997). Operational remote sensing of tropospheric aerosol over land from EOS moderate resolution imaging spectroradiometer. *J. Geophys. Res.*, 102, 17051-17067.
- Levy, R. C., L. Remer, S. Mattoo, E. Vermote, and Y. J. Kaufman (2007). Second-generation algorithm for retrieving aerosol properties over land from MODIS spectral reflectance. *J. Geophys. Res.*, 112, D13211, doi: 10.1029/2006JD007811.
- Li, X. and A. H. Strahler (1992). Geometric-optical bidirectional reflectance modeling of the discrete crown vegetation canopy: Effect of crown shape and mutual shadowing. *IEEE Trans. Geosci. Remote Sens.*, 30, 276-292.
- Lucht, W., and P. Lewis (2000). Theoretical noise sensitivity of BRDF and albedo retrieval from the EOS-MODIS and MISR sensors with respect to angular sampling. *Int. J. Rem. Sens.*, 21, 81-98.
- Lucht, W., Schaaf C. B., Strahler A. H. (2000). An algorithm for the retrieval of albedo from space using semiempirical BRDF models. *IEEE Trans. Geosci. Remote Sens.*, 38, 977-998.
- Lyapustin, A., and Yu. Knyazikhin, Green's function method in the radiative transfer problem. I: Homogeneous non-Lambertian surface (2001). *Appl. Optics*, 40, 3495-3501.
- Lyapustin, A., Y. Wang, R. Frey (2008). An Automatic Cloud Mask Algorithm Based on Time Series of MODIS Measurements. *J. Geophys. Res.*, 113, D16207, doi:10.1029/2007JD009641.
- Lyapustin, A., Y. Wang (2009). The Time Series Technique for Aerosol Retrievals Over Land from MODIS. pp. 69-99, in Satellite aerosol remote sensing over land, Eds. A. Kokhanovky and G. De Leeuw. Springer Praxis Books.
- Lyapustin, A., J. Martonchik, Y. Wang, I. Laszlo, S. Korkin (2011a). Multi-Angle Implementation of Atmospheric Correction (MAIAC): Part 1. Radiative Transfer Basis and Look-Up Tables. *J. Geophys. Res.*, 116, D03210, doi:10.1029/2010JD014985.

- Lyapustin, A., Y. Wang, I. Laszlo, R. Kahn, S. Korkin, L. Remer, R. Levy, and J. S. Reid (2011b). Multi-Angle Implementation of Atmospheric Correction (MAIAC): Part 2. Aerosol Algorithm. *J. Geophys. Res.*, 116, D03211, doi:10.1029/2010JD014986.
- Lyapustin, A., Y. Wang, I. Laszlo, and S. Korkin (2012). Improved cloud screening in MAIAC aerosol retrievals using spectral and spatial analysis. *Atmos. Meas. Tech.*, 5, 1-8, 2012, doi:10.5194/amt-5-1-2012.
- Moody, E. G., M. D. King, C. B. Schaaf, S. Platnick (2008). MODIS-Derived Spatially Complete Surface Albedo Products: Spatial and Temporal Pixel Distribution and Zonal Averages. *J. Appl. Meteor. Climatol.*, 47, 2879–2894.
- Pinty, B., M. Taberner, V. R. Haemmerle, S. R. Paradise, E. Vermote, M. M. Verstraete, N. Gobron, J.-L. Widlowski (2011). Global-Scale Comparison of MISR and MODIS Land Surface Albedos. *J. Climate*, 24, 732–749, doi: http://dx.doi.org/10.1175/2010JCL13709.1.
- Remer, L., Y. Kaufman, D. Tanre et al. (2005). The MODIS Aerosol Algorithm, Products, and Validation. *J. Atm. Sci.*, 62, 947-973.
- Roujean, J.-L., M. Leroy, and P. Y. Deschamps (1992). A bidirectional reflectance model of the Earth's surface for the correction of the remote sensing data. *J. Geophys. Res.*, 97, 20,455-20,468.
- Roy, D., P. Lewis and C. Justice (2002). Burned are mapping using multitemporal moderate spatial resolution data - a bi-directional reflectance model-based expectation approach. *Rem. Sens. Environ.*, 83, 263-286.
- Schaepman-Strub G., M. E. Schaepman, T. H. Painter, S. Dangel, J. V. Martonchik (2006). Reflectance quantities in optical remote sensing—definitions and case studies. *Remote Sensing Environ.*, 103 (1), 27–42.
- Schaaf C. B., Gao F., Strahler A.H., et al. (2002). First operational BRDF, albedo nadir reflectance products from MODIS. *Rem. Sens. Environ.*, 83, 135-148.
- Wang, Y., Lyapustin, A. I., Privette, J. L., Morisette, J. T., Holben, B. (2009). Atmospheric correction at AERONET locations: A new science and validation dataset. *IEEE Trans. Geosci. Remote Sens.*, 47:8, 2450-2466.
- Wang, Y., A. Lyapustin, J. Privette, R. Cook, S. K. SanthanaVannan, E. Vermote, and C. Schaaf (2010). Assessment of Biases in MODIS Surface Reflectance Due to Lambertian Approximation. *Rem. Sens. Environ.*, 114, 2791-2801, doi: 10.1016/j.rse.2010.06.013.
- Wolfe, R. E., Roy, D. P., and Vermote (1998). E. MODIS Land Data Storage, Gridding, and Compositing Methodology: Level 2 Grid. *IEEE Trans. Geosci. Remote Sens.*, 36, 1324–1338.

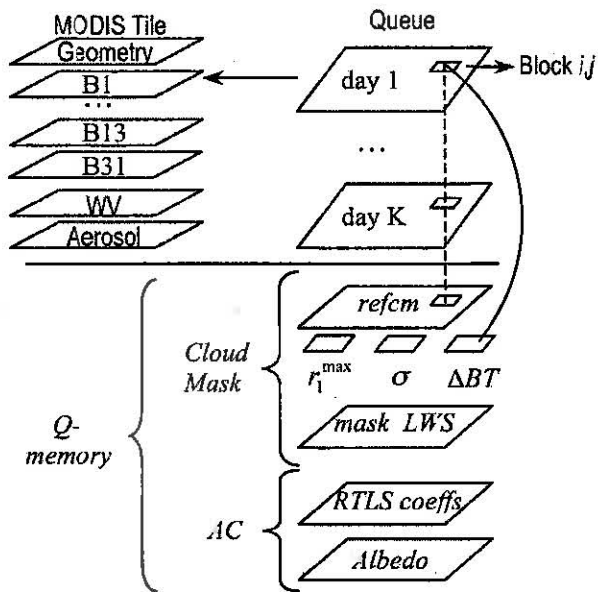


Figure 1. Structure of MAIAC Queue.

The Queue, designed for the sliding window algorithm, stores up to 16 days of gridded MODIS observations at 1 km resolution. The data are stored as Layers (double-indexed arrays) shown in the upper-left corner. A dedicated Q-memory is allocated to store the ancillary information for CM algorithm, such as a reference clear-skies image (*refcm*), block-level statistical parameters $\{r_{1_{max}}; \sigma; \Delta BT\}$, and results of dynamic Land-Water-Snow classification (*mask_LWS*). The Q-memory also stores results of previous reliable BRDF retrievals for MODIS bands 1-13.

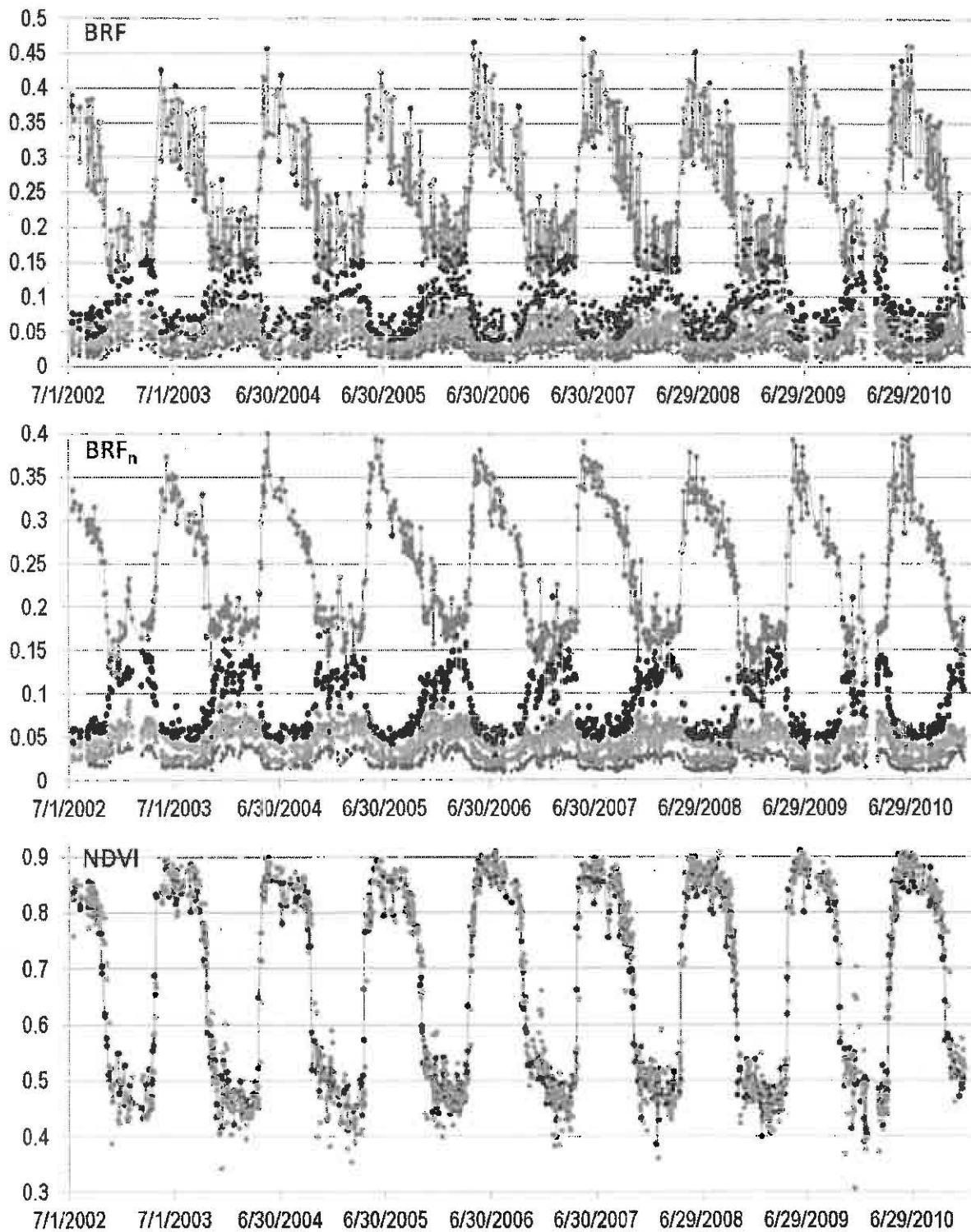


Figure 2. A time series of surface BRF (top), BRF_n (middle) and NDVI/NDVI_n (bottom) from MODIS Aqua data for a single 1 km pixel covered by a forest near Greenbelt, MD, USA. The BRF/BRF_n data are shown for 5 spectral bands: the red (B1), blue (B3) and green (B4) are indicated by their color, while NIR (B2) and SWIR (B7) are displayed in brown and back, respectively. At the bottom plot, the NDVI is shown in red, and NDVI_n is shown in black.

TOA CM NBRF BRF AOT CHNG TOA CM NBRF BRF AOT CHNG

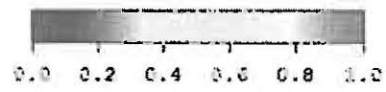
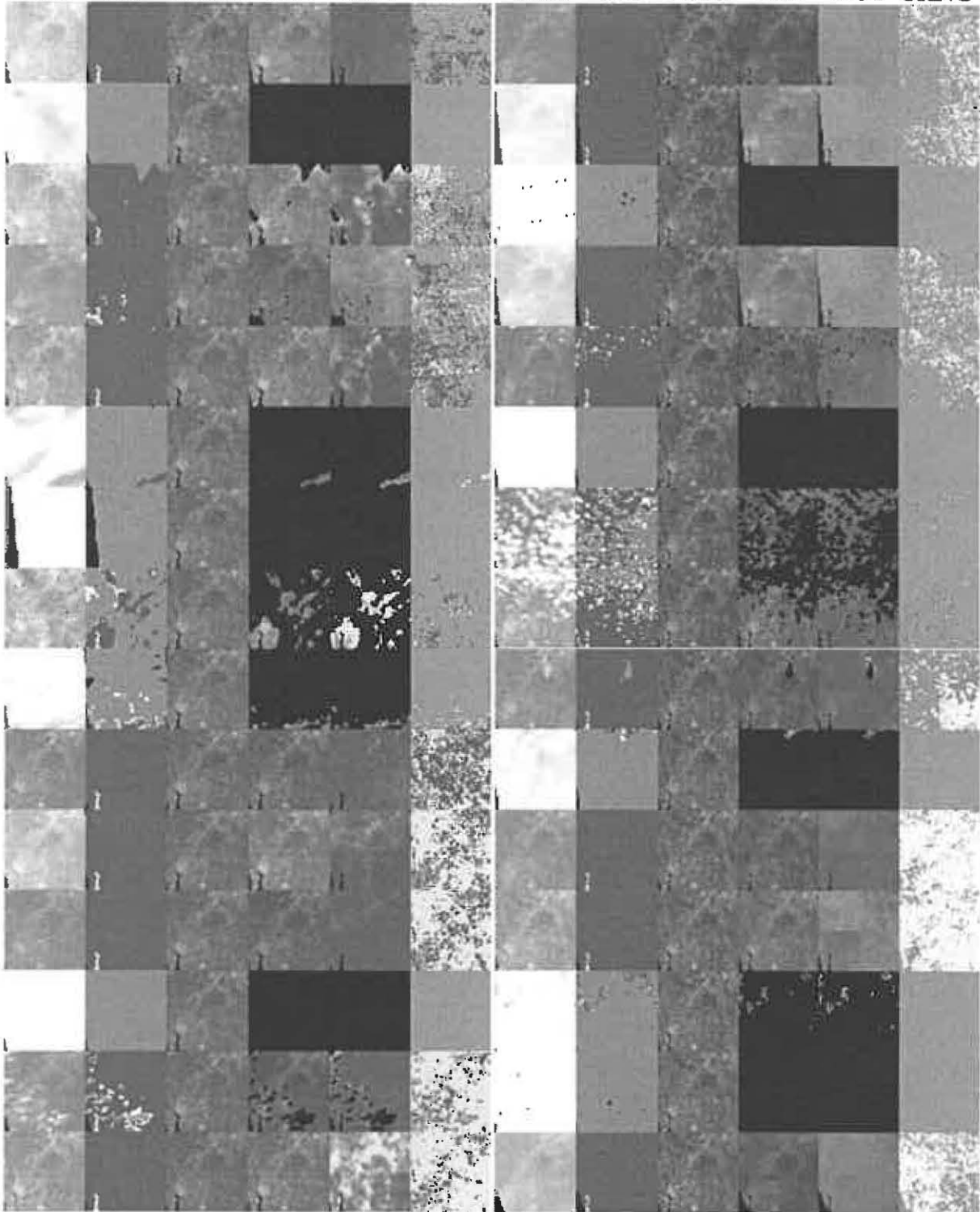


Figure 3. Illustration of MAIAC performance during spring green-up (left, DOY 92-105, 2010) and fall senescence (right, DOY 285-311, 2003) for 50 km MODIS Aqua subsets centered at NASA Goddard Space Flight Center, Maryland, USA. In each image, the vertical columns show: 1 - MODIS Aqua TOA RGB images; 2 - MAIAC CM (legend: red/yellow - cloud, blue/light blue - clear land/water); 3 - RGB NBRF; 4 - RGB BRF; 5 - MAIAC AOT at 0.466 μm with values in scale of 0-1; 6 - detected change (legend: pink - fill value; blue/green - $\text{_CHANGE/CHANGE_BIG}$ greening, cyan/yellow - $\text{_CHANGE/CHANGE_BIG}$ browning, red - discrepancy between the RTLS model and measured BRF in band B7 exceeds 3σ).

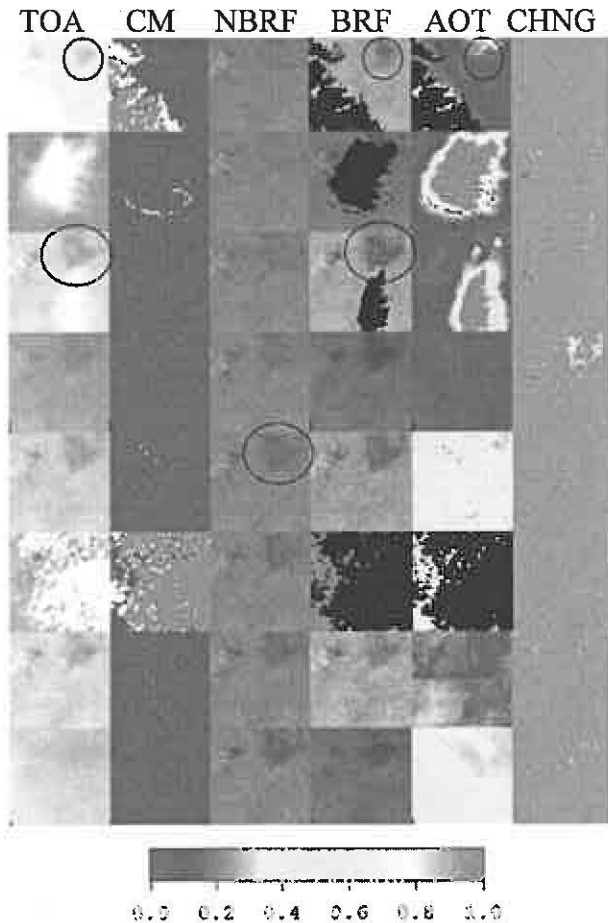
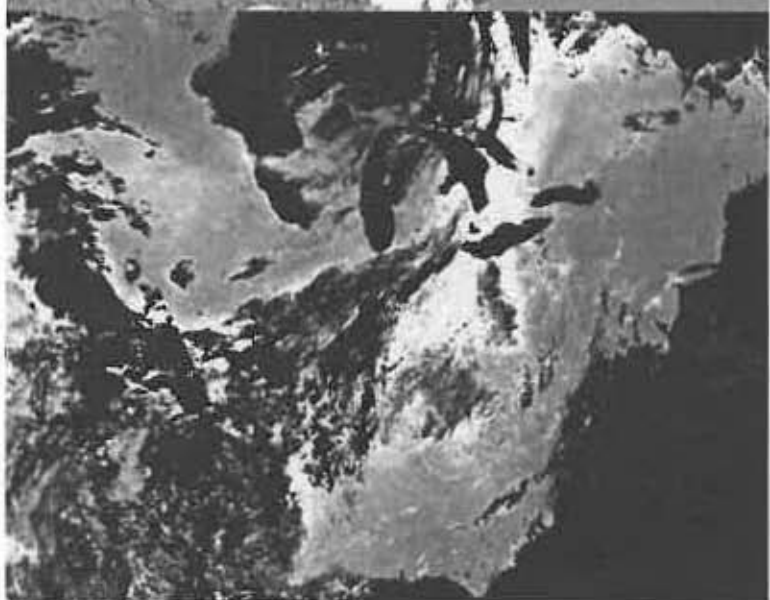
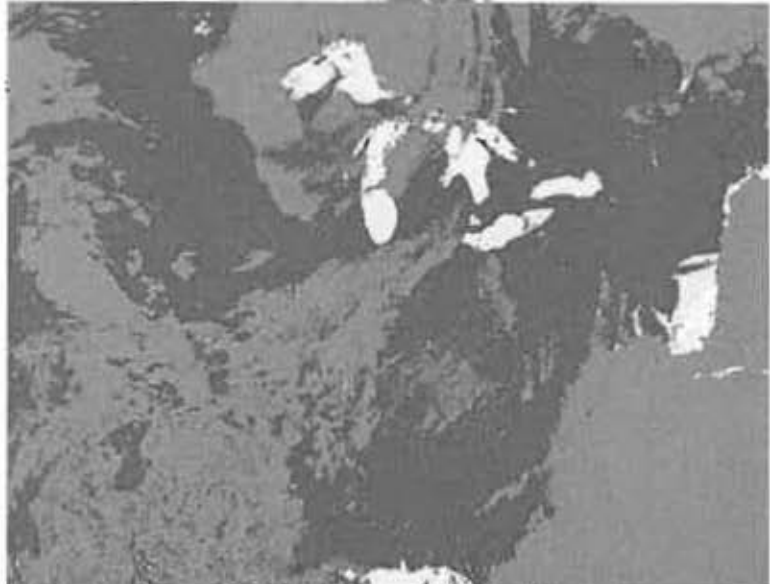


Figure 4. Rapid surface change caused by a fire near Skukuza, Africa. Columns and scales are the same as in Figure 3. The actively burning area (marked) becomes apparent immediately in the BRF images while the NBRF (BRDF model) response is delayed by 2 days.



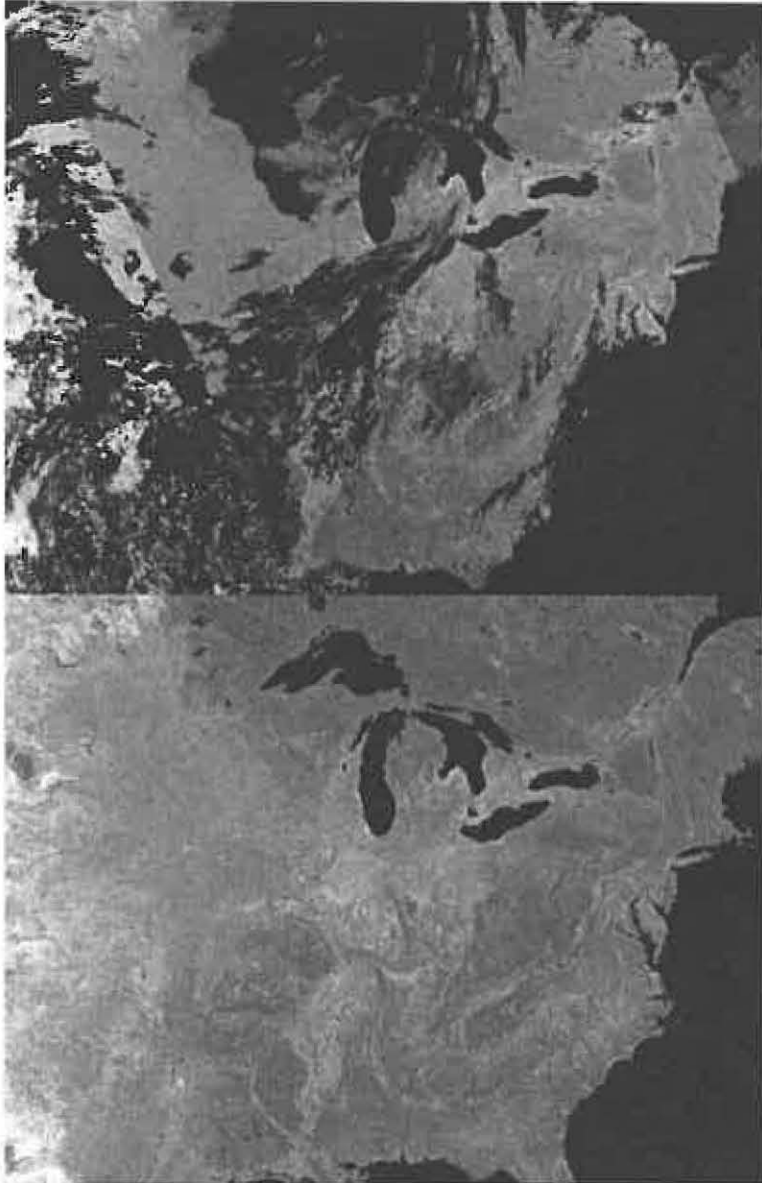


Figure 5. Example of MAIAC large scale processing for September 17, 2007. Shown from top are the TOA RGB MODIS Aqua image, MAIAC cloud mask, $AOT_{0.466}$, and RGB BRF and NBRF. The CM legend and a scale for AOT are given in caption of Figure 3.